Impact of a Regional US Drought on Land and Atmospheric Carbon

Eunjee Lee[1,2], Fan-Wei Zeng[2,3], Randal D. Koster[2], Lesley E. Ott[2], Sarith Mahanama[2,3], Brad Weir[1,2], Benjamin Poulter[4], and Tomohiro Oda[1,2]

1. Goddard Earth Sciences Technology and Research, Universities Space Research Association, Columbia, MD, USA
2. Global Modeling and Assimilation Office, NASA Goddard Space Flight Center, Greenbelt, MD, USA
3. Science Systems and Applications, Inc., Lanham, MD, USA
4. Biospheric Sciences Laboratory, NASA GSFC, Goddard Space Flight Center, MD, USA

Corresponding author: Eunjee Lee (eunjee.lee@nasa.gov)

Key points

- This study quantifies changes in meteorology and carbon caused by an idealized US drought (~500,000 km^2).
- Drought-area GPP decreases by 23% in the recovery month immediately after the drought while remote impacts on GPP are not spatially uniform.
- Drought-induced increase in column-averaged CO_2 of 0.78ppm is at the edge of the single sounding uncertainty of current GHG satellites.

Abstract

The impacts of drought on regional land and atmospheric carbon are still poorly understood. Here we quantify the impact of a regional US drought on land carbon fluxes (Gross Primary Production, or GPP, and Net Biosphere Production, or NBP) and atmospheric carbon (CO_2) by imposing an idealized 3-month meteorological drought in an ensemble of coupled land-atmosphere climate simulations. The imposed drought, applied to the lower Mississippi River Valley (~500,000 km^2), leads to a 23% GPP reduction in the drought area in the month immediately following the drought's termination. The drought also caused GPP reductions in some remote areas through drought-induced impacts on remote meteorology, particularly the areas adjacent to the imposed drought. In the remote areas, the induced precipitation changes are responsible for most of the anomalous land productivity. The impact of the drought-induced meteorological anomalies on GPP is greater than that of the CO_2 anomalies by at least an order of magnitude. While their impact on GPP is secondary, the drought-induced atmospheric CO_2 anomalies near the land surface can be as large as 3.57ppm. The significant CO_2 anomalies cover an area up to three times of that of the imposed drought, suggesting that atmospheric transport needs to be considered in the interpretation of drought-induced CO_2 anomalies in the atmosphere. The imposed drought also leads to column-averaged CO_2 increases of up to 0.78ppm, which is at the edge of the uncertainty from single soundings of current greenhouse gas (GHG) observing satellites.

Plain Language Summary

During a regional drought, a deficiency of precipitation affects vegetation productivity, which can alter net carbon exchange between the land and the atmosphere, and in turn, the CO_2 concentration in the atmosphere. Moreover, the anomalous heat and moisture fluxes at the land surface caused by the drought can generate changes in meteorology, affecting areas beyond the original drought area. Using a version of the NASA GEOS Earth System Model that allows full characterization of the carbon-water-energy feedback processes, we imposed an idealized spring drought over the lower Mississippi River Valley (~500,000 km^2) and quantified the resulting changes in vegetation productivity, net carbon exchange flux and atmospheric CO_2 concentration. We found that the productivity in the drought area decreases by 23% and that the productivities in some remote areas, particularly areas adjacent to the imposed drought, are also affected through impacts on remote meteorology. The anomalous atmospheric CO_2 caused by the idealized spring drought is at the edge of the measurement uncertainty of current greenhouse gas observing satellites. Due to atmospheric transport (e.g., wind), it covers an area up to three times of that of the imposed drought.

1 INTRODUCTION

A meteorological drought triggers anomalous hydrologic response at the land surface and in the atmosphere. The precipitation deficit reduces surface and root-zone soil water contents and, consequently, evapotranspiration, and this can lead to surface heat anomalies. These local environmental stresses can affect remote areas by perturbing the regional hydrological cycle (Koster et al., 2016) and delaying the rainy season onset (Shi et al., 2019). The soil moisture reduction and heat anomaly can also decrease vegetation activity, which can be observed by satellites as a decline of solar-induced chlorophyll fluorescence (SIF) and Normalized Difference Vegetation Index (NDVI), as in the case of the 2010 Russian drought (Yoshida et al., 2015). Overall land productivity and carbon sink capacity are accordingly affected (Schwalm et al., 2010).

Observational studies showing an impact of dryness and heat on carbon anomalies include a recent analysis of multiple measurements of the FLUXNET network (von Buttlar et al., 2018) and a study connecting anomalies of net land carbon exchange to the precipitation deficit in tropical South America during the strong 2015-2016 El Niño period (Liu et al., 2017). Modeling studies such as the Multi-scale Synthesis and Terrestrial Model Inter-comparison Project (MsTMIP) also estimated the range of the anomalous changes in terrestrial carbon productivities and fluxes in response to droughts (Zscheischler et al., 2014; Kolus et al., 2019). Net carbon anomalies in the inversion analyses that assimilated remotely sensed atmospheric CO_2 managed to infer drought signals (Liu et al., 2018; Byrne et al., 2019).

Recent US drought events (e.g., the 2011 TexMex drought and 2012 central US drought) demonstrate the complexity of the terrestrial ecosystem’s response to a regional drought (Parazoo et al., 2015; Sun et al., 2015; Wolf et al., 2016; Liu et al., 2018). During the year-long drought in the TexMex region in 2010/2011, during which the precipitation was reduced to less than half of the long-term mean value, the reduction in the regional summer carbon uptake was large enough to cause a negative anomaly in the annual total carbon uptake over the entire CONUS region (Parazoo et al., 2015). On the other hand, while the 2012 US central drought also led to a decrease in the summer carbon uptake, the relatively warmer spring of that year increased the spring carbon uptake, resulting in little change in the annual total carbon uptake (Wolf et al., 2016).

Disentangling the interactions between meteorological and carbon variations during and after a drought is a significant challenge, especially if one wants to account for two-way feedbacks between the land and the atmosphere. Modeling tools capable of simulating the feedback processes, e.g., Earth System Models (ESMs), allow us to explore such questions, since they integrate multiple facets of drought, including the impact of drought-induced stressors on ecosystems. Koster et al. (2016) imposed idealized meteorological droughts over 21 fractional areas in the US using the NASA Goddard Earth Observing System (GEOS) atmospheric general circulation model (AGCM) and quantified the resulting local and remote impacts on temperature and precipitation. They showed, for example, that a drought imposed in the lower Mississippi River Valley (part of the historical 2011 TexMex drought) can have impacts on temperature and precipitation in areas far outside the imposed drought.

The present study, in effect, builds on that of Koster et al. (2016) by adding a fully interactive carbon-cycle to their experiment – by allowing variations in water, energy, and carbon variables in both the land and the atmosphere to feedback on each other through a coupled treatment of the water, energy, and carbon cycles. We aim in particular to determine the magnitude and spatial extent of the temperature, precipitation, land carbon (GPP and NBP), and atmospheric carbon (CO_2) changes caused by an imposed regional US meteorological drought. The fully coupled cycles in the modeling system should allow an unprecedented examination of the feedbacks that may enhance or mitigate drought impacts on carbon fluxes.

Given the complexity of the problem, we employ a stepwise strategy. After describing our modeling tools and experimental methods, we demonstrate that the land model used responds sensibly to drought and is thus appropriate for this analysis; we do this by evaluating, against observation-based datasets, how well it reproduces the land carbon anomalies associated with a recent regional US drought event when driven offline with reanalysis meteorology. We then present results from two suites of coupled land-atmosphere ensemble simulations in which, for one of them, a 3-month, idealized regional drought is imposed in the lower Mississippi River Valley. Lastly, we isolate the impacts of the different induced meteorological anomalies (temperature, precipitation and atmospheric CO_2) on the terrestrial GPP anomalies using supplemental offline model simulations with forcing derived from the fully coupled simulations. We conclude with discussion and summary.

2 METHODS

2.1 Goddard Earth Observing System (GEOS) Model

We used the GEOS Earth System model maintained by the Global Modeling and Assimilation Office (GMAO) at the National Aeronautics and Space Administration's Goddard Space Flight Center (NASA GSFC). The GEOS model has been widely used to study various aspects of interactions among the Earth System components (e.g., Molod et al., 2012; Schubert et al., 2014; Koster et al., 2016; Wang et al., 2014). In this study, we used the Atmospheric General Circulation Model (AGCM) configuration (i.e., no coupled ocean component) in order to focus on the interactions between the atmosphere and the land ecosystem. In addition to the water and energy feedbacks between the land and the atmosphere already existing in the system, we have added for this analysis the carbon-cycle feedback, so that the model's prognostic atmospheric CO_2 can affect vegetation growth (and thus prognostic carbon reservoirs in the land) and simultaneously be affected by the model's net carbon exchange at the land surface. On the C90 cubed-sphere grid, which approximates a 1° latitude ×1° longitude grid, the transport of atmospheric CO_2 is computed with a time step of 15 minutes, including updates near the surface from fossil fuel emissions and CO_2 transfers across the atmosphere-land and atmosphere-ocean interfaces. The land carbon flux from the land component is updated every 3 hours.

The land carbon fluxes (e.g., GPP and NBP) are computed in this study by the process-based Catchment-CN terrestrial biosphere model. Catchment-CN is an extension of the original GEOS Catchment model, a hydrology-focused land surface model for simulating water and energy dynamics (Koster et al., 2000). Catchment-CN includes the terrestrial carbon-nitrogen (CN) dynamics contained within the National Center for Atmospheric Research (NCAR) Community Land Model version 4.0 (CLM4). The CLM4 routines allow Catchment-CN to follow carbon prognostic variables and compute a photosynthesis-based canopy conductance for the energy and water balance calculations, which still follow the strategy of the original Catchment model. Using time-steps of 7.5 minutes for energy and water dynamics and 90 minutes for carbon-nitrogen dynamics, the model provides simulated terrestrial carbon fluxes such as GPP, respiration, and NBP, the latter computed as:

$$\text{NBP} = \text{GPP} - \text{Ecosystem respiration} - \text{Fire} \tag{1}$$

The model carbon fluxes are computed using the environmental variables (temperature, precipitation, radiation, humidity, wind and atmospheric CO_2 listed in Table S1). More details on the Catchment-CN model can be found in Koster et al. (2014a) and Lee et al. (2018).

For our supplemental experiments run in stand-alone (offline) mode, the Catchment-CN model is forced by meteorological fields from NASA's Modern-Era Retrospective analysis for Research and Applications, version 2 (MERRA-2) dataset (Gelaro et al., 2017) and by surface CO_2 fields from NOAA's CarbonTracker (http://carbontracker.noaa.gov). The MERRA-2 meteorological fields (see Table S1 for details) have an hourly temporal resolution and a 0.5° latitude × 0.625° longitude spatial resolution. The MERRA-2 precipitation used in this study went through two additional correction processes: (1) it was first corrected with the gauge-based, global daily precipitation (the Climate Prediction Center Unified Gauge-based Analysis of Global Daily Precipitation, or CPCU), as described in Reichle et al. (2017a and 2017b); and (2) the corrected MERRA-2 precipitation from (1) was further scaled so that the background precipitation matches the climatology of the Global Precipitation Climatology Project, version 2.2 (GPCPv2.2) pentad precipitation. The NOAA CarbonTracker surface CO_2 has a 3-hourly temporal resolution and a 2° latitude × 3° longitude spatial resolution. Details on the spin-up process of the offline Catchment-CN are provided by Lee et al. (2018).

2.2 Observation-based datasets of drought-carbon connections

To evaluate GPP anomalies simulated by Catchment-CN offline, we used the FluxSat GPP product derived from MODerate-resolution Imaging Spectroradiometer (MODIS) surface reflectance data (Joiner et al., 2018). The offline model's NBP (see Equation 1) anomaly was compared to flux estimates from NOAA's CarbonTracker, version CT2017 (Peters *et al.,* 2007, with updates documented at http://carbontracker.noaa.gov), which were derived from *in situ* atmospheric CO_2 observations.

2.3 Experimental design and analysis metrics

2.3.1 Coupled AGCM simulations

We performed two suites of ensemble simulations using the GEOS AGCM. The simulations are free-running, meaning that they are informed by observed sea surface temperature (SST) distributions for a particular year but do not utilize any atmospheric data assimilation. Large numbers of simulations (i.e., large ensembles) with and without the imposed drought perturbation were run to separate the drought signal from internal atmospheric noise. The SST of year 2012 was applied to all simulations to minimize the influence of interannually-varying SSTs. Note, however, that while interannual SST variability was removed, the seasonal evolution of 2012 SST was retained.

Each ensemble suite consists of 45 simulations starting on April 1st and ending September 30th. The control suite (CTRL) allowed the land surface to receive the atmospheric model-produced precipitation over the entire simulation period. The drought suite (DROUGHT) applied an idealized, artificially imposed meteorological drought to a ~7° x ~7° area (on the C90 cubed-sphere grid, similar to 49 cells of 1° ×1° resolution) in the lower Mississippi River Valley (30-37N and 90-97W, see the grey area in Figure 1). The artificial drought was imposed from April 1st to June 30th; during this period, the model precipitation over the drought area was set to zero before it reached the land surface. The atmospheric variables responsible for generating precipitation were left unchanged. During the three-month recovery period that followed (July 1st through September 30th), the land surface received the model's precipitation, as in CTRL.

To provide a range of initial conditions for the 45 members of an ensemble suite, 15 members utilized the initial conditions that represent the land and atmospheric status of the MERRA-2 product on April 1st of each year during 2000 through 2014. Note that because 2012 SSTs were used in all simulations, the free-running simulations do not represent any particular year. The other 30 members of an ensemble used initial conditions constructed by applying slight atmospheric perturbations to the original 15 members (as in Koster et al., 2014b and Koster et al., 2016). All simulations were performed on the C90 cubed-sphere grid (~1° latitude ×1° longitude).

A z-score statistic was used to evaluate the significance of the drought-induced anomalies (Equation 2). σ is the standard deviation of the 45 values in the CTRL suite and N=45 is the number of ensemble members in each suite. The 95% confidence level ($p < 0.05$) was applied to determine the statistical significance of the anomalies.

$$z = \frac{\overline{(\overline{DROUGHT} - \overline{CTRL})}}{\frac{\sigma}{\sqrt{N}}} \quad (2)$$

2.3.2 Offline Catchment-CN simulations using the coupled model meteorology

After completing the full coupled ensemble simulations, we conducted additional offline simulations in which the stand-alone Catchment-CN model was driven by different combinations of the (archived) meteorological and surface CO_2 fields generated in the coupled simulations. These offline simulations are designed to quantitatively isolate the effect of the different drought-induced atmospheric anomalies on land-carbon fluxes.

In the baseline run of the offline simulations, we used the monthly temperature and precipitation climatologies (2000-2014) of MERRA-2 and AGCM CTRL simulations to scale the hourly MERRA-2 temperature and precipitation forcing. In essence, through the scaling, the monthly temperature and precipitation climatologies of the hourly offline baseline meteorological forcing were forced to match those of the AGCM CTRL simulations. By doing so, the offline baseline simulations mimic the AGCM CTRL simulations. We then performed four offline experiments using the temperature, precipitation, and surface CO_2 written out during the AGCM DROUGHT experiments:

EXP_{T2M}: same as the baseline but AGCM CTRL 2-meter air temperature (T2M) climatology was replaced by that from the AGCM DROUGHT experiments;

EXP_{PRCP}: same as the baseline but AGCM CTRL precipitation (PRCP) climatology was replaced by that from the AGCM DROUGHT experiments, with the drought area again receiving zero precipitation during April 1 - June 30;

EXP_{CO2}: the monthly surface CO_2 anomalies (AGCM DROUGHT minus AGCM CTRL) were added to the NOAA CarbonTracker CO_2 forcing which was used in the baseline run, and

EXP_{ALL}: all of the forcing changes in EXP_{T2M}, EXP_{PRCP}, and EXP_{CO2} were employed.

The baseline and the four experiments each consisted of 15 simulations (each simulation taking forcing and land surface initial conditions from a different year in 2000-2014) and was six months long (April through September) to match the coupled AGCM simulations. A fully spun-up Catchment-CN simulation driven by MERRA-2 meteorology and NOAA CarbonTracker atmospheric CO_2 provided the April 1 land surface initial conditions used in these offline simulations. The contribution of drought-induced meteorological or CO_2 changes to terrestrial GPP was analyzed in terms of the simulated GPP anomaly (EXP GPP minus baseline GPP).

3 RESULTS

3.1 Evaluation of the offline model's response to a US drought

We first evaluate the response of the offline Catchment-CN model to a historical US drought: the central US drought of 2011. The simulated land carbon anomalies (GPP and NBP), as produced by the model when driven with MERRA-2 reanalysis meteorology and CarbonTracker CO_2, are compared here to the observation-based GPP (FluxSat) and NBP (CT2017) products.

Overall, the Catchment-CN's GPP anomalies agree well with FluxSat GPP anomalies (Joiner et al., 2018) during the 2011 TexMex drought. The observed negative anomalies during April through June (AMJ, Figure 2a), as well as the strong negative anomalies in the southern US during the July through September (JAS) period (Figure 2b), are well reproduced by the Catchment-CN. Over CONUS as a whole (24N-50N, 125W-67W), the simulated GPP anomalies (-0.08 PgC for AMJ and -0.05 PgC for JAS) agree well with the FluxSat GPP anomalies (-0.07 PgC for AMJ and -0.02PgC for JAS).

The spatial pattern of the simulated NBP anomalies during AMJ (top graph in Figure 2c) reflects the pattern of the simulated GPP anomalies (Figure 2a) and agrees reasonably well with the anomaly pattern of CT2017 NBP (bottom graph in Figure 2c). During JAS, the negative NBP anomaly in the TexMex area is less dispersed than the CT2017 anomaly (Figure 2d). As CT2017 uses the first-guess (*a priori*) land fluxes based on the Carnegie-Ames Stanford Approach (CASA) biogeochemical models (CASA-GFED 4.1s and CASA_CMS) (CarbonTracker Team, 2018) for the atmospheric inversion, the differences in the mechanistic representations between the Catchment-CN model and the CASA model can introduce a difference in the spatial pattern. The sign and magnitude of model NBP anomalies over CONUS (-0.08 PgC during AMJ and -0.05 PgC during JAS) are comparable to the CT2017 estimates (-0.03 PgC during AMJ and -0.02 PgC during JAS).

GPP anomalies show better agreement with the observation-based product than do NBP anomalies presumably because the model GPP responds directly to a given meteorological forcing whereas the model NBP calculation includes other carbon fluxes such as respiration and fire (Equation 1) that introduce additional uncertainties. The poorer agreement between model NBP and CT2017-based NBP may also reflect some deficiencies in the performance of the CT product. For example, the interannual variability of net carbon flux during recent drought events was not well captured in the previous version (CT2016); the summer net carbon flux anomalies in the northern extratropics did not show a good correlation with temperature anomalies and a drought index (Byrne et al., 2019). Note that the comparisons in Figure 2 can be considered representative; a corresponding evaluation of the model's ability to capture GPP and NBP anomalies during the 2012 central US drought shows similar model performance (Figure S1).

3.2 Results of an idealized drought experiment

By performing the idealized drought experiments with the atmospheric GEOS model as described in Section 2.1, we can estimate drought-induced land carbon anomalies (GPP and NBP) and atmospheric CO_2 anomalies in the context of coupled energy, water, and carbon cycles.

3.2.1 Localized impact in the area of imposed drought

Figure 3 shows the 2-meter air temperature (T2M) and carbon anomalies from the coupled ensemble simulations (DROUGHT minus CTRL). The impact of the imposed drought over the drought area is summarized in Figure 4. The drought caused T2M to increase in the drought area by up to 1°C (Figures 3a and 4a). More importantly, the largest positive temperature anomaly occurs in July (+1K or +0.3%, $p < 0.05$) after we stopped artificially imposing the meteorological drought, which demonstrates the drought's extended temporal impact. This warm temperature anomaly continues throughout the entire recovery period (July through September) and is statistically significant at $p < 0.05$ (Figure 4a). Precipitation anomalies in the drought area do not appear to be statistically significant during the recovery period, except for the month (July) immediately after the drought ends (-0.2 mm/day or -13% reduction in July, also see Figure 4b). The soil moisture at the land surface and in the root-zone is significantly ($p < 0.05$) reduced by the drought (Figures 4c and 4d), and the impact continues during the recovery period, particularly for the root-zone soil moisture (Figure 4d); the reduction of evapotranspiration through this reduced soil moisture presumably explains the positive temperature anomalies.

The land carbon fluxes (e.g., GPP and NBP) in the drought area and the atmospheric CO_2 are significantly impacted by the drought-induced air temperature and soil moisture anomalies. Indeed, the drought's extended effect during the recovery period manifests itself particularly strongly in the carbon anomalies (Figures 4e, 4f, 4g and 4h). The drought-induced GPP reductions are strong: the last drought month (June) shows a -11.8% reduction, and even larger reductions are seen during recovery (-23.1% in July, -21.0% in August, and -13.7% in September; all statistically significant at $p < 0.05$; see Figure 4e). The negative NBP anomalies (meaning that the land is a smaller carbon sink or a larger carbon source) in the drought area are significant ($p < 0.05$), starting from the second month of the drought period and persisting through recovery period. The drought also causes an earlier transition of the NBP seasonality. Under the normal climate (i.e. CTRL), the land ecosystem in this area shifts from being a carbon sink to a carbon source between July and August. The imposed drought causes the transition to occur one month earlier than usual (Figure 4g). Lastly, the drought induces positive anomalies of surface CO_2 ($p < 0.05$, Figure 4h); these correspond to the aforementioned negative NBP anomalies (Figures 3c and 3d).

3.2.2 Impact in remote regions

The meteorological anomalies generated by a drought through land-atmosphere feedback need not be strictly local; anomalies can be translated to remote areas through atmospheric transport, and even the nature of the transport itself may be modified by the local anomalies (Koster et al. 2016). Here we examine the drought-induced anomalies in the six remote areas immediately adjacent to the drought area (Figure 1).

In the west and east remote regions, the positive T2M anomalies induced by the drought are statistically significant ($p < 0.05$) during the drought period. This does not, however, translate to significant GPP changes there in May and June (Figure 3b); while the June GPP anomalies, for example, are generally consistent with the June T2M anomalies (e.g., along the Gulf Coast), they are simply less spatially extensive. The negative NBP anomaly and the positive surface CO_2 anomaly in the east are statistically significant during the drought period. In the southwest remote region, the land and atmospheric carbon anomalies are all statistically significant ($p < 0.05$) during the drought period, but the changes are relatively small (Table 1), as the regional productivity there is relatively low.

Interestingly, positive atmospheric CO_2 anomalies are statistically significant ($p < 0.05$) in most remote areas: in N, W, E and SW during the drought period (Table 1), and in N, NE, W and SW during the recovery period (Table 2). In particular, the surface CO_2 anomaly increases by up to 0.66 ppm in N during the recovery period (Table 2), indicating a delayed response of the terrestrial ecosystem to the drought. Moreover, this region's surface CO_2 anomaly is statistically significant while its NBP anomaly is not, which suggests that the CO_2 anomaly is induced, at least partially, by advected CO_2 anomalies from the drought region. Overall, the general increase in surface CO_2 across much of CONUS in Figure 3d illustrates the role of atmospheric transport (i.e., by wind) of anomalous surface CO_2 from the region of imposed drought to remote areas.

3.3 Isolating the contribution of different drought-induced anomalies to GPP

Through land-atmosphere feedback, the imposed drought in our experiment has impacts on local and remote air temperature, precipitation, and atmospheric CO_2 throughout the simulations. Changes in each of these fields can in turn feedback on the simulated land carbon fluxes. How important are these feedbacks? Is it possible, for example, that the drought-induced increases in atmospheric CO_2 can “fertilize” to some extent the remote vegetation? To isolate the strengths of the different feedbacks, we performed the additional offline Catchment-CN simulations described in Section 2.3.2. In essence, the drought-induced T2M, precipitation and atmospheric CO_2 anomalies generated in the coupled ensemble simulations above were applied separately to the land surface in the offline ensembles, and the resulting simulated GPP was compared to that of the offline control ensemble.

Results are shown in Figure 5. In the area of imposed drought, the drought-induced positive temperature anomalies by themselves contribute to a GPP reduction (-4.1% during the drought period and -12.2% during the recovery period; see Figure 5a). The majority of the GPP reduction in the drought area (-92.4% during the drought period and -88.0% during the recovery period), however, is attributable to precipitation changes (Figure 5b). The positive surface CO_2 anomalies in the atmosphere do act as a very slight fertilizer to the vegetation (Figure 5c); the GPP increases are indeed very small, an order of magnitude smaller than the decreases induced by the precipitation and air temperature anomalies. Note that the sum of the contributions of temperature, precipitation and surface CO_2 anomalies to GPP changes is close to that obtained when all three forcing changes are applied simultaneously (Figure 5d, showing changes that are 96.1% of the sum of Figures 5a, b, and c, during the drought period and 99.8% during the recovery period), suggesting that the impacts of these chosen meteorological anomalies on GPP are essentially independent of each other.

Considering the six remote areas outlined in Figure 1, the precipitation anomaly by itself causes a slight increase in GPP directly to the north (Figure 5b), roughly compensating for about 4.4% of the GPP decrease seen in the drought area. On the other hand, the precipitation-induced GPP anomalies in the west, east and southwest are all negative (Figure 5b). In fact, in the east, the precipitation-induced GPP reduction is roughly 10% of that seen in the drought area itself during the recovery period – the dryness impacts of the imposed drought extend not only temporally after the drought ends but also spatially, in a significant way.

Remote temperature impacts on GPP appear negligible. Remote surface CO_2 impacts are always positive (i.e., the CO_2 fertilization effect) but the increment is very slight (Figure 5c). In neither local nor remote regions are the increases in surface CO_2 significant enough to compensate for the GPP reductions caused by lower water availability.

4 DISCUSSION AND CONCLUSIONS

Our study provides a unique look at the joint evolution of energy, water and carbon anomalies induced by an imposed regional drought. Through a land-atmosphere modeling system featuring coupled energy, water, and carbon cycles, we show that imposing an idealized drought within a 7° x 7° area (~500,000 km^2) in the lower Mississippi River Valley for three months produces impacts on land and atmospheric carbon that extend well beyond this area and time period. The response of the terrestrial carbon cycle to the imposed drought lags behind the drought by one or two months, consistent with the lag times seen in a previous study using multiple offline land carbon models in MsTMIP (Kolus et al., 2019). This delayed response may be even longer in reality (Kolus et al., 2019), and it can, in turn, cause slower vegetation recovery (i.e., drought legacy effect) in forest ecosystems (Anderegg et al., 2015). The spatial extent of the drought's impact on land carbon anomalies is largely limited to the areas adjacent to the imposed drought (Figure 3); areas farther away are not so affected (Figure S2).

Through supplemental offline experiments, this study also quantifies the isolated impact of drought-induced meteorological anomalies (temperature, precipitation and atmospheric CO_2) on terrestrial GPP. Over the course of the drought and recovery periods, the GPP in remote areas is mostly affected by precipitation anomalies (~90%). While the spatial extent of the positive atmospheric CO_2 anomalies induced by the drought is large (Figure 3d), their impact on GPP is at least an order of magnitude smaller than that of the meteorological anomalies. The marginal impact of this drought-induced CO_2 "fertilization" in the fully coupled system, though not unexpected, is nevertheless (to our knowledge) quantified here for the first time.

Note that we are assuming here a resilient terrestrial ecosystem; the drought is not allowed to induce a permanent change in land cover type. Our coupled ensemble simulations, which are designed to illustrate the overall land-atmospheric response to an idealized regional drought at time scales out to 6 months, do not address longer term impacts. The timing and frequency of actual drought(s) occurring (perhaps episodically) over longer periods may result in an ecosystem transition from one state to another state (for example, forest conversion to grasslands). This may lead to a greater impact of drought through atmospheric teleconnections (Swann et al., 2018), or result in a different fate of the land ecosystem (Sippel et al., 2016).

In the course of our analysis, we considered the hypothesis that drought-induced reductions in leaf area index (LAI) might reduce evapotranspiration after the (meteorological) drought ends. The reduced evapotranspiration sink might allow precipitation to fill the soil column faster and thereby might speed soil moisture recovery. That is, drought-induced degradations of vegetation might actually contribute to faster drought recovery times. Using the offline model, we examined soil moisture deficit recovery following drought termination in a simulation with appropriately degraded LAI against that in a simulation using climatological LAI. Changes in soil moisture recovery time were found to be essentially negligible. This, however, should be considered a preliminary result; future work is necessary to pin down more carefully the effect of drought-induced LAI changes on soil moisture recovery time.

A major advantage of using a coupled model over an offline model in a study of drought impacts is the direct simulation of the atmospheric CO_2 concentration; this allows us to avoid having to estimate and interpret drought-induced CO_2 variations via other, presumably indirect, means. It also allows us to account directly for the effect of atmospheric transport on the spatial translation of drought-induced signals. Explicitly including the carbon feedback between the land and the atmosphere and the effect of dynamic phenology on the meteorology should, in principle, yield a more realistic simulation of the evolution of drought over its onset, maintenance, and recovery periods.

The drought-induced CO_2 anomalies at the surface level, averaged over a month, can be as large as 3.57ppm (Figure S3a) (or 1.5ppm averaged over the drought area in July – one month after the drought termination). An observation-based study focusing on drought impacts on CO_2 provides some basis for comparison. During the 2010 Amazon drought, the positive CO_2 anomalies at four aircraft sample sites were reported to range from 2 to 4 ppm (Gatti et al., 2014; see their Figures 3a-d), comparable to the surface CO_2 anomalies simulated here. We note, however, that another study (Peters et al., 2018) uses isotope measurements to suggest that Earth system models in general may underestimate the actual impact of drought on carbon uptake.

On the other hand, the drought-induced anomalies of the column-averaged CO_2 (i.e., total moles CO_2 divided by total moles wet air) are up to 0.78 ppm (Figure S3b). This value is the monthly anomaly within a particular grid cell in July and August, the months immediately following the termination of the artificial drought. While our column CO_2 does not represent exactly the same variable as the column-averaged dry air mole fraction of atmospheric CO_2 (X_{CO2}), which the carbon observing satellites such as the Greenhouse gases Observing Satellite (GOSAT) and Orbiting Carbon Observatory 2 (OCO-2) actually measure, these simulated and satellite-measured variables are similar enough to warrant comparison. While the maximum value of the column CO_2 anomaly in our experiments is smaller than a single sounding uncertainty estimate (~1ppm) of the OCO-2 satellite (Eldering et al., 2017), it is greater than the systematic bias of 0.6ppm found by Kulawik et al. (2019). Note that the error characteristics of the carbon observing satellite measurements remain an active area of research and that the OCO-2 error characteristics change with subsequent versions of the NASA Atmospheric CO_2 Observations from Space (ACOS) X_{CO2} retrieval algorithm (Kiel et al., 2019; Kulawik et al., 2019; O'Dell et al., 2018). Based on the available observational error estimates, our simulation results suggest that the impact of a spring drought of this size (~500,000 km^2) on atmospheric carbon is at the edge of the uncertainty levels associated with single soundings of the carbon observing satellites in operation.

One caveat about our study regards our use of the same (2012) SST field in every simulation. While this was done to simplify our interpretation of the results, we note that simulated drought impacts (particularly remote impacts) may have been different under different SST conditions (e.g., under different El Niño–Southern Oscillation states). SST in the Gulf of Mexico could play a very important role in regional and large-scale dynamics and transport. For example, in summer, the regional wind pattern in the southern US is dominated by wind that blows in from the Gulf of Mexico after passing over the Atlantic Ocean. Different SSTs in the Gulf could either amplify or dampen the temperature gradient between the land and the ocean, which could alter the teleconnection pattern and thereby affect the regional monsoon. The potential impact of inter-annually varying SST conditions on carbon-related drought impacts requires further study.

Atmospheric transport does appear to play an important role in extending spatially the impacts of a local drought on atmospheric CO_2. The aforementioned land-ocean temperature gradient should be enhanced by drought-induced warming, which could intensify the onshore sea breeze. We see some hints of this impact in our results: the northern part of the drought region and the adjacent remote regions to the north show positive anomalies of surface CO_2 in June and July, whereas the southern part of the drought region shows negative anomalies in August and September (Figure 3d). Our ongoing work is in fact aimed at isolating and quantifying the separate effects of land carbon flux variability and atmospheric transport variability on the variability of atmospheric CO_2.

Acknowledgements

This work was supported by the NASA GMAO core grant. The authors thank Yehui Chang, Rolf Reichle, Jana Kolassa, Huisheng Bian, and Young-Kwon Lim for their comments and suggestions. We also thank two anonymous reviewers for their helpful comments. The CarbonTracker (CT2017) data was provided by NOAA ESRL in Boulder, Colorado, USA (http://carbontracker.noaa.gov). NASA GMAO's MERRA-2 reanalysis meteorology is available at the MERRA-2 project page (https://gmao.gsfc.nasa.gov/reanalysis/MERRA-2/). The FluxSat GPP is available at https://avdc.gsfc.nasa.gov/.

References

Anderegg, W. R. L., Schwalm, C., Biondi, F., Camarero, J. J., Koch, G., Litvak, M., et al. (2015). Pervasive drought legacies in forest ecosystems and their implications for carbon cycle models. *Science*, *349*(6247), 528–532. https://doi.org/10.1126/science.aab1833

Byrne, B., Jones, D. B. A., Strong, K., Polavarapu, S. M., Harper, A. B., Baker, D. F., & Maksyutov, S. (2019). On what scales can GOSAT flux inversions constrain anomalies in terrestrial ecosystems? *Atmospheric Chemistry and Physics*, *19*(20), 13017–13035. https://doi.org/10.5194/acp-19-13017-2019

CarbonTracker Team. (2018, June 5). CarbonTracker Documentation CT2017 release. Retrieved from https://www.esrl.noaa.gov/gmd/ccgg/carbontracker/CT2017_doc.php#tth_sEc2

Eldering, A., O'Dell, C. W., Wennberg, P. O., Crisp, D., Gunson, M. R., Viatte, C., et al. (2017). The Orbiting Carbon Observatory-2: first 18 months of science data products. *Atmospheric Measurement Techniques*, *10*(2), 549–563. https://doi.org/10.5194/amt-10-549-2017

Gatti, L. V., Gloor, M., Miller, J. B., Doughty, C. E., Malhi, Y., Domingues, L. G., et al. (2014). Drought sensitivity of Amazonian carbon balance revealed by atmospheric measurements. *Nature*, *506*(7486), 76–80. https://doi.org/10.1038/nature12957

Gelaro, R., McCarty, W., Suárez, M. J., Todling, R., Molod, A., Takacs, L., et al. (2017). The Modern-Era Retrospective Analysis for Research and Applications, Version 2 (MERRA-2). *Journal of Climate*, *30*(14), 5419–5454. https://doi.org/10.1175/JCLI-D-16-0758.1

Joiner, J., Yoshida, Y., Zhang, Y., Duveiller, G., Jung, M., Lyapustin, A., et al. (2018). Estimation of Terrestrial Global Gross Primary Production (GPP) with Satellite Data-Driven Models and Eddy Covariance Flux Data. *Remote Sensing*, *10*(9), 1346. https://doi.org/10.3390/rs10091346

Kiel, M., O'Dell, C. W., Fisher, B., Eldering, A., Nassar, R., MacDonald, C. G., & Wennberg, P. O. (2019). How bias correction goes wrong: measurement of X_{CO2} affected by erroneous surface pressure estimates. *Atmospheric Measurement Techniques*, *12*(4), 2241–2259. https://doi.org/10.5194/amt-12-2241-2019

Kolus, H. R., Huntzinger, D. N., Schwalm, C. R., Fisher, J. B., McKay, N., Fang, Y., et al. (2019). Land carbon models underestimate the severity and duration of drought's impact on plant productivity. *Scientific Reports*, *9*(1). https://doi.org/10.1038/s41598-019-39373-1

Koster, R. D., Suarez, M. J., Ducharne, A., Stieglitz, M., & Kumar, P. (2000). A catchment-based approach to modeling land surface processes in a general circulation model: 1. Model structure. *Journal of Geophysical Research*, *105*(D20), 24809. https://doi.org/10.1029/2000JD900327

Koster, R. D., Walker, G. K., Collatz, G. J., & Thornton, P. E. (2014a). Hydroclimatic Controls on the Means and Variability of Vegetation Phenology and Carbon Uptake. *Journal of Climate*, *27*(14), 5632–5652. https://doi.org/10.1175/JCLI-D-13-00477.1

Koster, R. D., Chang, Y., & Schubert, S. D. (2014b). A Mechanism for Land–Atmosphere Feedback Involving Planetary Wave Structures. *Journal of Climate*, *27*(24), 9290–9301. https://doi.org/10.1175/JCLI-D-14-00315.1

Koster, R. D., Chang, Y., Wang, H., & Schubert, S. D. (2016). Impacts of Local Soil Moisture Anomalies on the Atmospheric Circulation and on Remote Surface Meteorological Fields during Boreal Summer: A Comprehensive Analysis over North America. *Journal of Climate*, *29*(20), 7345–7364. https://doi.org/10.1175/JCLI-D-16-0192.1

Kulawik, S. S., Crowell, S., Baker, D., Liu, J., McKain, K., Sweeney, C., et al. (2019). Characterization of OCO-2 and ACOS-GOSAT biases and errors for CO2 flux estimates. *Atmos. Meas. Tech. Discuss.*, *2019*, 1–61. https://doi.org/10.5194/amt-2019-257

Lee, E., Zeng, F.-W., Koster, R. D., Weir, B., Ott, L. E., & Poulter, B. (2018). The impact of spatiotemporal variability in atmospheric CO_2 concentration on global terrestrial carbon fluxes. *Biogeosciences*, *15*(18), 5635–5652. https://doi.org/10.5194/bg-15-5635-2018

Liu, J., Bowman, K. W., Schimel, D. S., Parazoo, N. C., Jiang, Z., Lee, M., et al. (2017). Contrasting carbon cycle responses of the tropical continents to the 2015–2016 El Niño. *Science*, *358*(6360), eaam5690. https://doi.org/10.1126/science.aam5690

Liu, J., Bowman, K., Parazoo, N. C., Bloom, A. A., Wunch, D., Jiang, Z., et al. (2018). Detecting drought impact on terrestrial biosphere carbon fluxes over contiguous US with satellite observations. *Environmental Research Letters*, *13*(9), 095003. https://doi.org/10.1088/1748-9326/aad5ef

Molod, A., Takacs, L., Suarez, M., Bacmeister, J., Song, I.-S., & Eichmann, A. (2012). The GEOS-5 Atmospheric General Circulation Model: Mean Climate and Development from MERRA to Fortuna, Technical Report Series on Global Modeling and Data Assimilation, Volume 28, NASA/TM–2012-104606.

O'Dell, C. W., Eldering, A., Wennberg, P. O., Crisp, D., Gunson, M. R., Fisher, B., et al. (2018). Improved retrievals of carbon dioxide from Orbiting Carbon Observatory-2 with the version 8 ACOS algorithm. *Atmospheric Measurement Techniques*, *11*(12), 6539–6576. https://doi.org/10.5194/amt-11-6539-2018

Parazoo, N. C., Barnes, E., Worden, J., Harper, A. B., Bowman, K. B., Frankenberg, C., et al. (2015). Influence of ENSO and the NAO on terrestrial carbon uptake in the Texas-northern Mexico region. *Global Biogeochemical Cycles*, *29*(8), 1247–1265. https://doi.org/10.1002/2015GB005125

Peters, W., Jacobson, A. R., Sweeney, C., Andrews, A. E., Conway, T. J., Masarie, K., et al. (2007). An atmospheric perspective on North American carbon dioxide exchange: CarbonTracker. *Proceedings of the National Academy of Sciences*, *104*(48), 18925–18930. https://doi.org/10.1073/pnas.0708986104

Peters, W., van der Velde, I. R., van Schaik, E., Miller, J. B., Ciais, P., Duarte, H. F., et al. (2018). Increased water-use efficiency and reduced CO2 uptake by plants during droughts at a continental scale. *Nature Geoscience*, *11*(10), 744–748. https://doi.org/10.1038/s41561-018-0212-7

Reichle, R. H., Liu, Q., Koster, R. D., Draper, C. S., Mahanama, S. P. P., & Partyka, G. S. (2017a). Land Surface Precipitation in MERRA-2. *Journal of Climate*, *30*(5), 1643–1664. https://doi.org/10.1175/JCLI-D-16-0570.1

Reichle, R. H., Draper, C. S., Liu, Q., Girotto, M., Mahanama, S. P. P., Koster, R. D., & De Lannoy, G. J. M. (2017b). Assessment of MERRA-2 land surface hydrology estimates. *Journal of Climate*. https://doi.org/10.1175/JCLI-D-16-0720.1

Schubert, S. D., Wang, H., Koster, R. D., Suarez, M. J., & Groisman, P. Ya. (2014). Northern Eurasian Heat Waves and Droughts. *Journal of Climate*, *27*(9), 3169–3207. https://doi.org/10.1175/JCLI-D-13-00360.1

Schwalm, C. R., Williams, C. A., Schaefer, K., Arneth, A., Bonal, D., Buchmann, N., et al. (2010). Assimilation exceeds respiration sensitivity to drought: A FLUXNET synthesis. *Global Change Biology*, *16*(2), 657–670. https://doi.org/10.1111/j.1365-2486.2009.01991.x

Shi, M., Liu, J., Worden, J. R., Bloom, A. A., Wong, S., & Fu, R. (2019). The 2005 Amazon Drought Legacy Effect Delayed the 2006 Wet Season Onset. *Geophysical Research Letters*, *46*(15), 9082–9090. https://doi.org/10.1029/2019GL083776

Sippel, S., Zscheischler, J., & Reichstein, M. (2016). Ecosystem impacts of climate extremes crucially depend on the timing. *Proceedings of the National Academy of Sciences*, *113*(21), 5768–5770. https://doi.org/10.1073/pnas.1605667113

Sun, Y., Fu, R., Dickinson, R., Joiner, J., Frankenberg, C., Gu, L., et al. (2015). Drought onset mechanisms revealed by satellite solar-induced chlorophyll fluorescence: Insights from two contrasting extreme events, *Journal of Geophysical Research: Biogeosciences*, *120*(11), 2427–2440. https://doi.org/10.1002/2015JG003150

Swann, A. L. S., Laguë, M. M., Garcia, E. S., Field, J. P., Breshears, D. D., Moore, D. J. P., et al. (2018). Continental-scale consequences of tree die-offs in North America: identifying where forest loss matters most. *Environmental Research Letters*, *13*(5), 055014. https://doi.org/10.1088/1748-9326/aaba0f

von Buttlar, J., Zscheischler, J., Rammig, A., Sippel, S., Reichstein, M., Knohl, A., et al. (2018). Impacts of droughts and extreme-temperature events on gross primary production and ecosystem respiration: a systematic assessment across ecosystems and climate zones. *Biogeosciences*, *15*(5), 1293–1318. https://doi.org/10.5194/bg-15-1293-2018

Wang, H., Schubert, S., Koster, R., Ham, Y.-G., & Suarez, M. (2014). On the Role of SST Forcing in the 2011 and 2012 Extreme U.S. Heat and Drought: A Study in Contrasts. *Journal of Hydrometeorology*, *15*(3), 1255–1273. https://doi.org/10.1175/JHM-D-13-069.1

Wolf, S., Keenan, T. F., Fisher, J. B., Baldocchi, D. D., Desai, A. R., Richardson, A. D., et al. (2016). Warm spring reduced carbon cycle impact of the 2012 US summer drought. *Proceedings of the National Academy of Sciences*, *113*(21), 5880–5885. https://doi.org/10.1073/pnas.1519620113

Yoshida, Y., Joiner, J., Tucker, C., Berry, J., Lee, J.-E., Walker, G., et al. (2015). The 2010 Russian drought impact on satellite measurements of solar-induced chlorophyll fluorescence: Insights from modeling and comparisons with parameters derived from satellite reflectances. *Remote Sensing of Environment*, *166*, 163–177. https://doi.org/10.1016/j.rse.2015.06.008

Zscheischler, J., Michalak, A. M., Schwalm, C., Mahecha, M. D., Huntzinger, D. N., Reichstein, M., et al. (2014). Impact of large-scale climate extremes on biospheric carbon fluxes: An intercomparison based on MsTMIP data. *Global Biogeochemical Cycles*, *28*(6), 585–600. https://doi.org/10.1002/2014GB004826

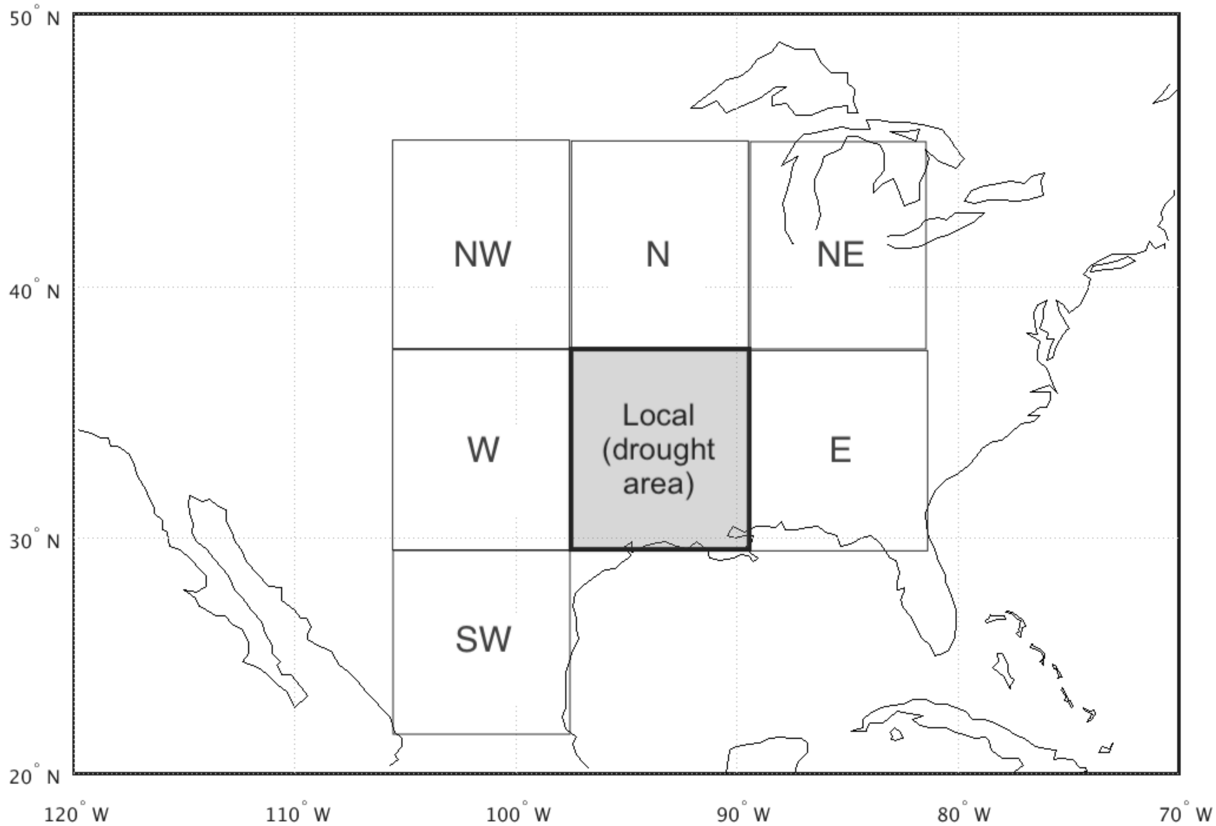

Figure 1. Domain of the imposed regional drought in the US (grey area of ~500,000 km^2, located at 30N-37N and 90W-97W). In the DROUGHT suite, model-generated precipitation within the grey area was set to zero for April, May and June, but was retained for July, August, and September. Six equal areas adjacent to the local drought are chosen to study the remote impact of the drought.

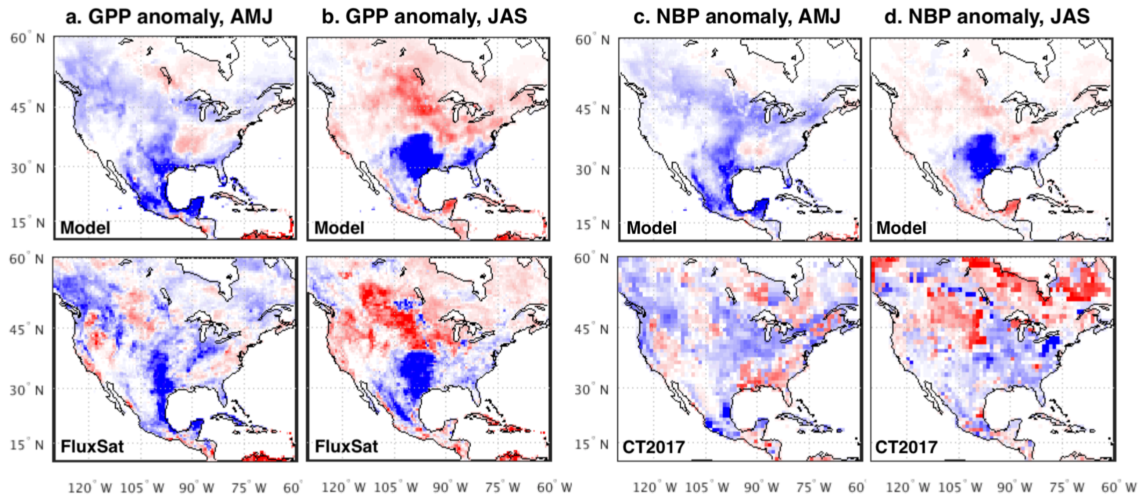

Figure 2. Model and observed GPP anomalies during (a) April-May-June (AMJ) and (b) July-August-September (JAS) during the 2011 TexMex drought. NBP anomalies are shown in (c) and (d). The anomalies were computed as the value for 2011 relative to the 14-year (2003-2016) climatology.

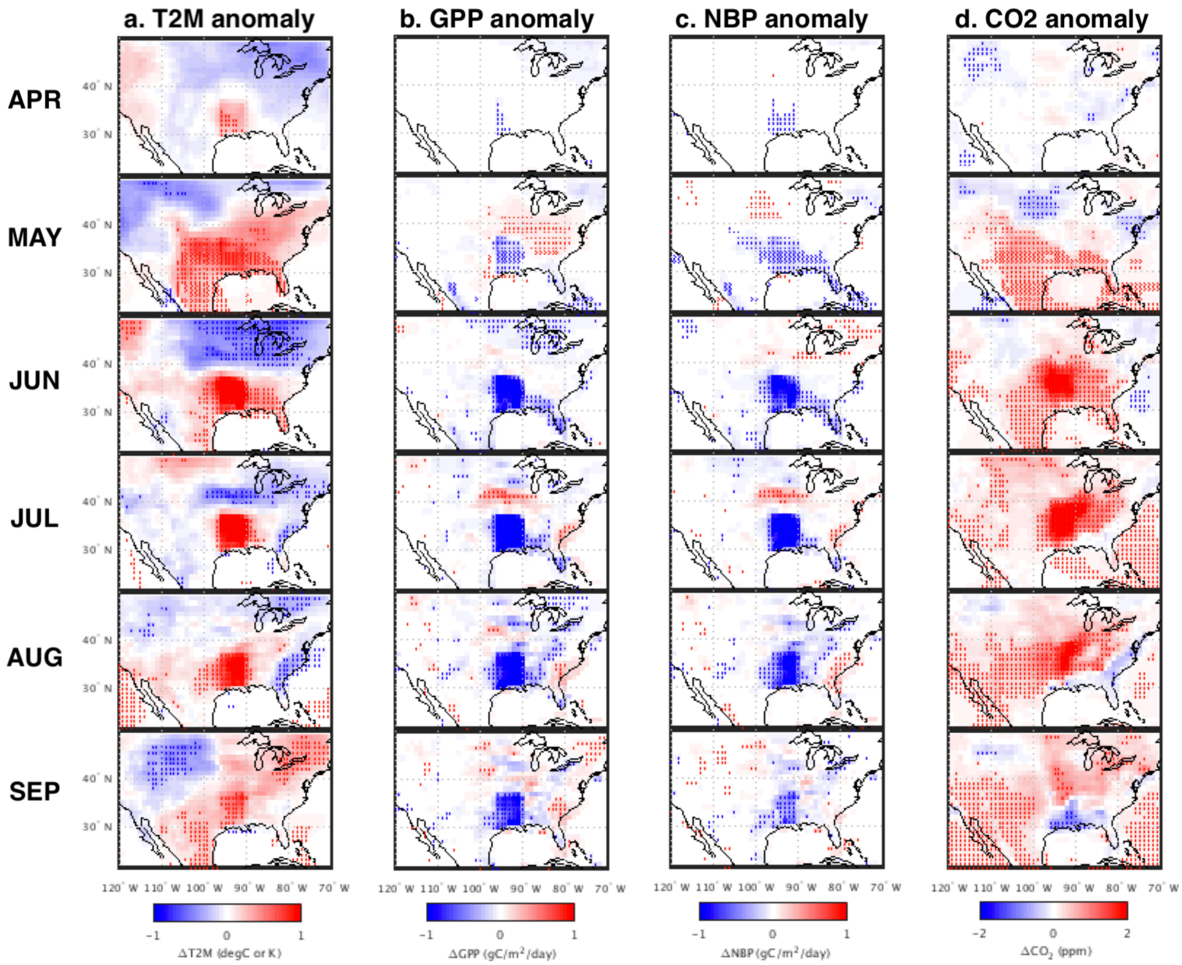

Figure 3. Monthly anomalies (DROUGHT minus CTRL) caused by the imposed drought: (a) T2M (°C), (b) GPP (gC/m^2/day), (c) NBP (gC/m^2/day), and (d) surface CO_2 (ppm) in the lowest atmospheric model layer (about 50m). Hatched areas indicate the anomalies that are statistically significant with $p < 0.05$. Note that the drought period is from April to June, followed by the 3-month recovery period from July to September.

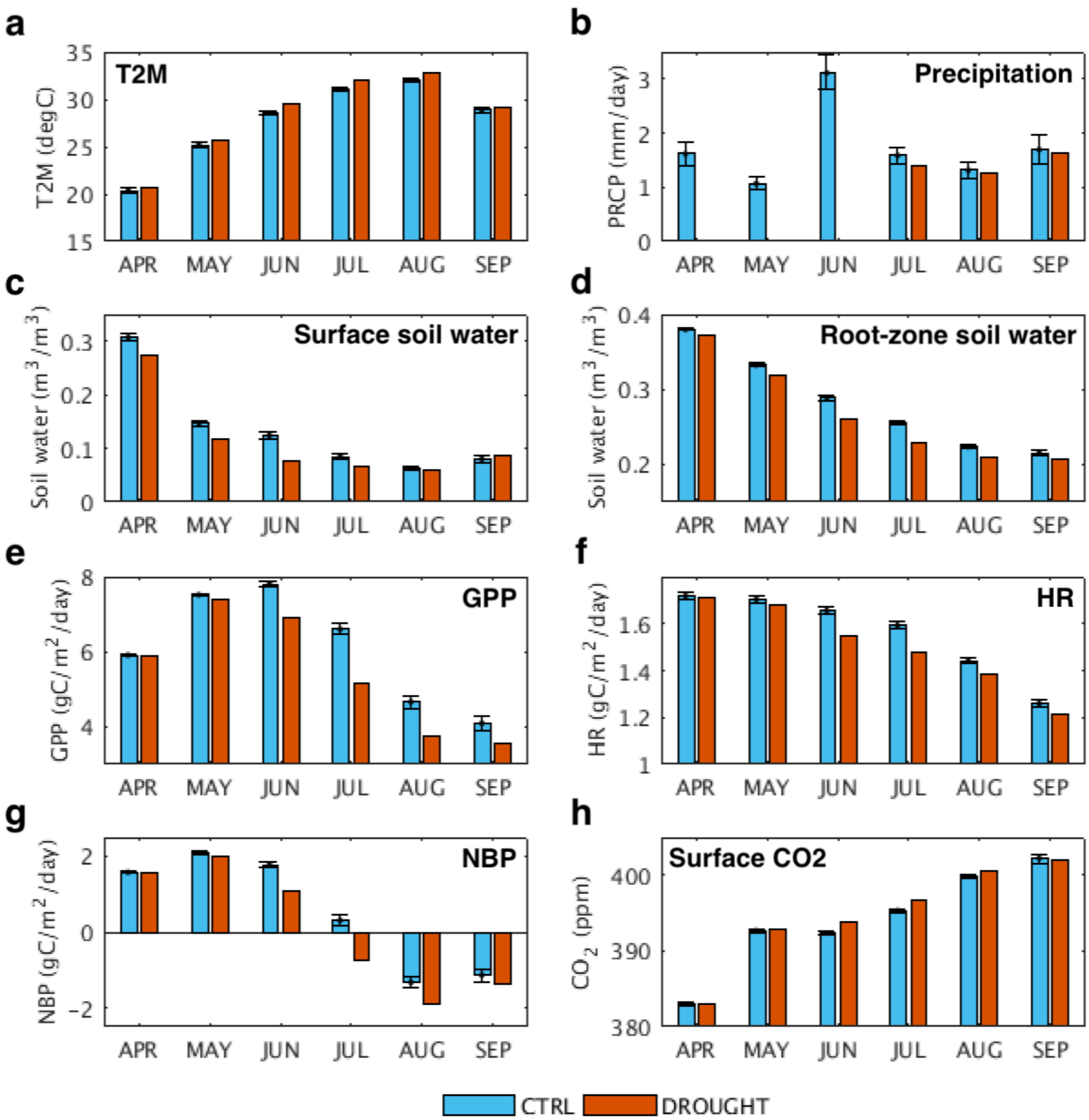

Figure 4. Mean monthly values of (a) T2M (°C), (b) PRCP (mm/day), (c) Surface soil water (m^3/m^3), (d) Root-zone soil water (m^3/m^3), (e) GPP ($gC/m^2/day$), (f) heterotrophic respiration ($gC/m^2/day$), (g) NBP ($gC/m^2/day$), and (h) surface CO_2 (ppm) in the area of imposed drought during the drought (April-May-June) and the recovery period (July-August-September) (Blue: CTRL; Red: DROUGHT). A red bar being higher (lower) than the upper (lower) limit of the paired blue bar's error ranger indicates that the change is statistically significant at $p < 0.05$.

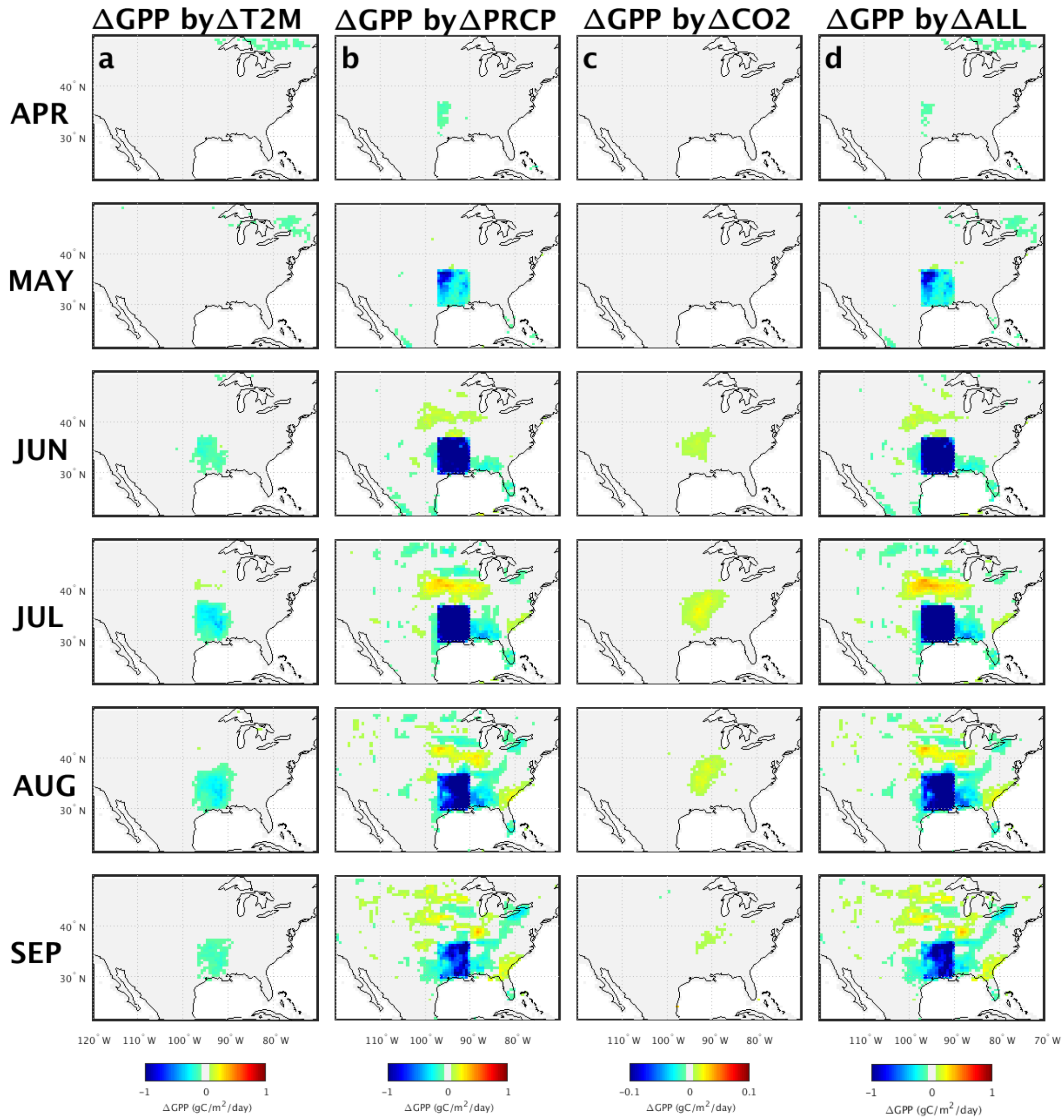

Figure 5. Contributions of isolated drivers to GPP as determined in supplemental experiments with the offline Catchment-CN model. The isolated contributions of drought-induced (a) T2M, (b) PRCP and (c) surface CO_2 anomalies to GPP are shown (note a different scale in c). The GPP anomalies in (d) indicate the anomalies from the combined contribution of T2M, PRCP and CO_2 anomalies.

Drought	ΔT2M (°C)	ΔGPP (gC/m^2/day)	ΔNBP (gC/m^2/day)	ΔCO_2 (ppm)
Drought area	+0.6	-0.342	-0.278	+0.53
NW	-0.2	+0.009	+0.016	-0.02
N	-0.1	+0.014	+0.012	+0.17
NE	-0.1	-0.002	+0.007	+0.10
W	+0.2	-0.011	-0.028	+0.31
E	+0.2	-0.013	-0.037	+0.22
SW	+0.1	-0.004	-0.003	+0.03

Table 1. Mean anomalies of T2M (°C), GPP (gC/m^2/day), NBP (gC/m^2/day), and surface CO_2 (ppm) in the drought area and six remote areas during the drought period (April-May-June). The remote areas are adjacent to the drought area, as illustrated in Figure 1. The anomalies shown are for DROUGHT minus CTRL, and the shaded values are statistically significant at $p < 0.05$.

Recovery	ΔT2M (°C)	ΔGPP ($gC/m^2/day$)	ΔNBP ($gC/m^2/day$)	ΔCO_2 (ppm)
Drought area	+0.7	-0.968	-0.620	+0.70
NW	-0.1	+0.029	+0.018	+0.25
N	+0.01	-0.001	-0.024	+0.66
NE	+0.01	-0.006	-0.018	+0.55
W	+0.1	-0.029	-0.023	+0.37
E	+0.1	-0.075	-0.038	+0.19
SW	0.0	-0.003	-0.002	+0.03

Table 2. Mean anomalies of T2M (°C), GPP ($gC/m^2/day$), NBP ($gC/m^2/day$), and surface CO_2 (ppm) in the drought area and the six remote areas during the recovery period (July-August-September). The remote areas are adjacent to the drought area, as illustrated in Figure 1. The anomalies shown are for DROUGHT minus CTRL, and the shaded values are statistically significant at $p < 0.05$.